JOURNAL OF GUIDANCE, CONTROL, AND DYNAMICS
Vol. 30, No. 4, July–August 2007

Adaptive Output Feedback Control of a Flexible Base Manipulator

Bong-Jun Yang,* Anthony J. Calise,† and James I. Craig‡
Georgia Institute of Technology, Atlanta, Georgia 30332

DOI: 10.2514/1.23707

This paper considers augmentation of an existing inertial damping mechanism by neural network-based adaptive control, for controlling a micromanipulator that is serially attached to a macromanipulator. The approach is demonstrated using an experimental test bed in which the micromanipulator is mounted at the tip of a cantilevered beam that resembles a macromanipulator with its joint locked. The inertial damping control combines acceleration feedback with position control for the micromanipulator so as to simultaneously suppress vibrations caused by the flexible beam while achieving precise tip positioning. Neural network-based adaptive elements are employed to augment the inertial damping controller when the existing control system becomes deficient due to modeling errors and uncertain operating conditions. There were several design challenges that had to be faced from an adaptive control perspective. One challenge was the presence of a nonminimum phase zero in an output feedback adaptive control design setting in which the regulated output variable has zero relative degree. Other challenges included flexibility in the actuation devices, lack of control degrees of freedom, and high dimensionality of the system dynamics. In this paper we describe how we overcame these difficulties by modifying a previous augmenting adaptive approach to make it suitable for this application. Experimental results are provided to illustrate the effectiveness of the augmenting approach to adaptive output feedback control design.

I. Introduction

FLEXIBLE-LINK manipulators are often used in industrial robotics where a lightweight and long-reach capability is needed, such as in space robotics [1,2], nuclear maintenance [3], and waste storage tank remediation [4]. A typical problem in long-reach manipulators is that flexible links are susceptible to low-frequency vibrations induced by movement of the robot itself or by external disturbances and are difficult to control due to low stiffness. For example, it is reported that a large portion of the operation time of a remote manipulator system was spent waiting for vibrations to decay before a real task is initiated [5,6]. Therefore, a great deal of research has been devoted to reducing settling time by suppressing vibrations in the flexible links, and numerous control methods have been developed during the past two decades [7,8].

Control strategies for flexible manipulator systems are typically classified as feedforward (open loop) or feedback (closed loop) control schemes [8]. The method of input shaping belongs to the class of feedforward controllers that focuses on minimizing vibrations induced by the robot itself and suppresses unwanted vibration by determining trajectories that avoid or minimize vibration [1,9–12]. However, it is not well suited for rejecting external disturbances. On the other hand, feedback control techniques use measurements and estimation of system states to reduce vibrations [8] and offer the potential for attenuating the influence of external disturbances. Various feedback methods have been used and adapted to flexible manipulator systems [7]. References [7,8] provide a survey for both feedforward and feedback controllers. Approaches that combine input shaping with feedback controllers have also been proposed in [13–16], in which shaped commands are tracked by feedback controllers.

A macro/micromanipulator is a specialized robotic system comprising a large flexible arm with a short-reach rigid manipulator attached to its end. This configuration was first introduced by Sharon and Hogan [17] for applications that require long-reach capability, together with fine dexterous manipulation [18]. Because its long-reach capability is provided by a flexible arm, as is the case for general flexible manipulators, achieving fine tip positioning within acceptable time in general necessitates the design of a control system that provides damping for vibrations in the macromanipulator. An initial attempt in this direction was to design controllers separately for the macro- and the microsubsystems [17]. However, undesirable interactions were observed when the gains on the microcontroller are large [19]. When the reference input to the micromanipulator is formed as a difference between the desired tip position and the macromanipulator endpoint position so as to improve inertial tip positioning, the analysis in [20] shows that the resulting control architecture creates a feedback loop between the two subsystems, and designing independent controllers for the macro- and microsubsystems can result in system instability, therefore putting a limitation on the decoupled controller designs for a macro/micromanipulator.

Inertial damping control is an approach that uses a micromanipulator to produce inertial interactions that damp the vibrations of the macromanipulator, with additional sensors engaged to measure vibrations in the macromanipulator. To avoid the design of a single concurrent controller, the rigid links and the flexible links are regulated by independent controllers assuming that their dynamics are separated in time scales. This method has been applied by many researchers [14,21–29] and proven effective in experimental studies. In particular, various tests were performed by Book and his colleagues at Georgia Tech [26–29] using the test bed located in the Intelligent Machine Dynamics Laboratory (IMDL), in which a micromanipulator, SAMII (Small Articulated Manipulator II), is mounted at the tip of a cantilevered beam fixed to the ceiling, the base motion of which is similar to that at the tip of a flexible manipulator with locked joints. In general, however, the design of an inertial damping controller requires a relatively accurate model for the interactions between the micromanipulator and the base, which is essential to avoid particular locations where coupling effects

Presented as Paper 5322 at the AIAA Guidance, Navigation, and Control Conference, Providence, RI, 16–19 August 2004; received 7 March 2006; revision received 27 February 2007; accepted for publication 1 March 2007.

*Research Engineer II, School of Aerospace Engineering; jun.yang@ae.gatech.edu. Member AIAA.
†Professor, School of Aerospace Engineering; anthony.calise@ae.gatech.edu. Fellow AIAA.
‡Professor, School of Aerospace Engineering; james.craig@ae.gatech.edu. Senior Member AIAA.

between the micromanipulator and the base are not suitable for vibration damping [30]. In the design, it is important to limit the control gain to ensure that model uncertainties do not lead to instabilities. Also, it is important to maintain a proper link configuration so that inertial effects dominate the interaction forces [18,30].

In this paper, we employ a neural network (NN)-based adaptive control design to augment the existing inertial damping controller that may be deficient due to either inherent uncertainties in the interactions between the rigid links and the flexible link or uncertain operating conditions. In [29], it is shown how modal uncertainty associated with the macromanipulator dynamics can lead to instabilities similar to those observed in [20]. For simplicity of analysis, in [29] an inertial damping controller is applied to damp the vibrations in the base using only a single link while the other joints are only regulated in their position, and a root locus analysis is performed with experimental transfer functions obtained in a single configuration. To study the use of adaptive control for robustifying an inertial damping controller, we incorporate NN-based adaptive control to augment the controller given in [29].

It is well established that a NN can approximate any continuous function to any desired accuracy on a compact domain [31]. This universal approximation property has been used in adaptive control [32–35], and its potential for controlling uncertain flexible systems has been illustrated with simulation and experimental studies [36–38]. Its applications for robot manipulators are addressed in a state feedback setting in [32,33,39]. In [40–45], the NN-based approach has been further extended to output feedback. Especially, the approaches in [42–45] have been developed in a control architecture in which adaptive control augments an existing linear controller. This form is particularly advantageous for this application due to the presence of the existing inertial damping controller. The difference between the approach in [42] and that in [43–45] is the methodology by which the adaptive elements are designed. Although the adaptive elements are designed based on inversion in [42], those in [43–45] do not rely on inversion and can be applied to nonminimum phase systems. Even for minimum phase systems, inversion based control is not recommended when the system contains lightly damped modes.

In this paper the adaptive element is designed following the methods described in [43–45], because regulating acceleration by moving the micromanipulator renders the system nonminimum phase. This is often the case when flexible-link robot arms are controlled by noncollocated actuators and sensors ([46], pp. 20–26). The main challenges (beyond the nonminimum phase aspect of the problem) in applying the adaptive method in [43–45] for this application include zero relative degree of the regulated output variable, significant flexibility in the actuation devices [47,48], and a lack of control degrees of freedom (the system treated combines both position control and vibration control in a *single* input design setting). Furthermore, the system dynamics used in the existing design included the second mode of base vibration, which adds an additional degree of complexity to the augmenting adaptive design. Thus one significant contribution of this paper is to detail how these nonstandard forms, arising due to dynamic features of the flexible manipulator regulated by the existing inertial damping control, were handled by modifying the method in [43–45].

The paper is organized as follows: In Sec. II we describe the essential features of the IMDL test bed in a linear setting. The existing inertial damping controller and the challenges induced by the existing control system design when we attempt to augment with the adaptive control are addressed in Sec. III. Emphasis is placed on how the approach in [43] was modified and on how the resulting adaptive design can be reformulated for as being performed for a nonminimum phase system having relative degree equal to one. Next, the theoretical aspect of designing an augmenting adaptive controller for a system having relative degree one is presented in Sec. IV. The specific details of the adaptive control augmentation in this application are given in Sec. V. Experimental results are described to support the validity of the overall approach in Sec. VI. Conclusion are presented in Sec. VII, and a stability analysis is provided in the Appendix.

Throughout the manuscript, $\|\cdot\|$ denotes the Euclidean norm for a vector and the induced 2-norm for a matrix unless otherwise mentioned. That is, $\|\boldsymbol{x}\| = \sqrt{\boldsymbol{x}^T\boldsymbol{x}}$ for $\boldsymbol{x} \in \mathbb{R}^n$, and $\|A\| = \sqrt{\lambda_{\max}(A^TA)}$ for $A \in \mathbb{R}^{m\times n}$.

II. System Description

Figure 1 depicts SAMII mounted serially to a 5-m long cantilevered beam suspended vertically from an I-beam in the ceiling of the lab. The actuators of the system are hydraulic servomotors at the joints of SAMII. These are rotary vane actuators with electrohydraulic servovalves. Optical encoders located on the shaft of each joint perform measurement of the rotational position of the joints. For vibration control, base accelerations are measured by accelerometers located at the beam tip. Figure 1b defines the coordinates related to the control design. With the definitions given in Fig. 1b, the configuration in Fig. 1a is described by $\theta_1 = -90$ deg, $\theta_2 = 90$ deg, and $\theta_3 = 90$ deg, and $x = 0$, which represents the initial position where the control system starts. The existing control system considers only vibration control in a single direction (x) by implementing an inertial damping controller to a single link (link 2), while the other links and the wrist are under decoupled position control. Therefore, only the variable θ_2 among joint angles is used in design of the control system, and the notation θ is used in place of θ_2 throughout the paper.

The hydraulic actuator model [29], a linear model derived by curve fitting experimental data obtained with the configuration as shown in Fig. 1a, is as follows:

$$\frac{\theta}{u} = P_\theta(s) = \frac{K_1[(s/\omega_2)^2 + 2\zeta_2(s/\omega_2) + 1]}{s(s/\tau + 1)[(s/\omega_p)^2 + 2\zeta_p(s/\omega_p) + 1]} \tag{1}$$

where θ is in degrees, and u is the input voltage to the hydraulic servovalve for the joint angle θ_2. The parameters in this model are the following: $K_1 = 20$, $\omega_p = 8.2$ Hz, $\zeta_p = 0.11$, $\omega_2 = 10$ Hz, $\zeta_2 = 0.06$, $\tau = 30$ Hz. Figure 2 compares the frequency response of the model in Eq. (1) to that of experimental data. Note that the model in (1) includes flexibility in the actuator model, in contrast to that in [26,30].

In the same manner, the acceleration of the base is derived as a transfer function by curve fitting. This linear model implies that the Coriolis term and centrifugal forces are assumed negligible in the interaction forces (a procedure for a detailed nonlinear analytical

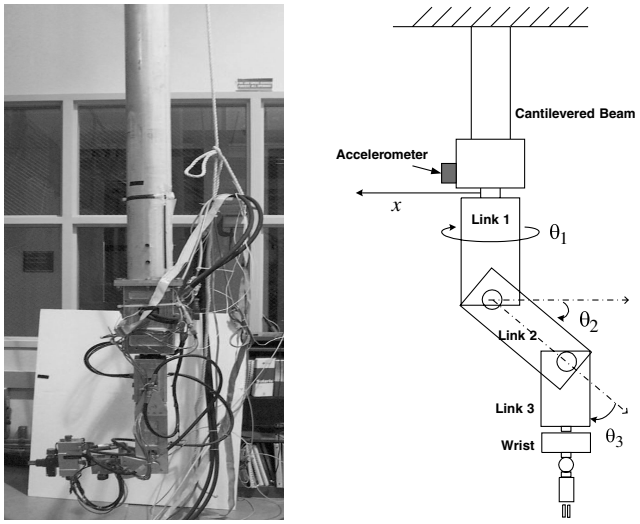

a) b)

Fig. 1 a) Test bed at the Intelligent Machine Dynamics Laboratory at Georgia Tech. b) Definitions of coordinates in the existing control system.

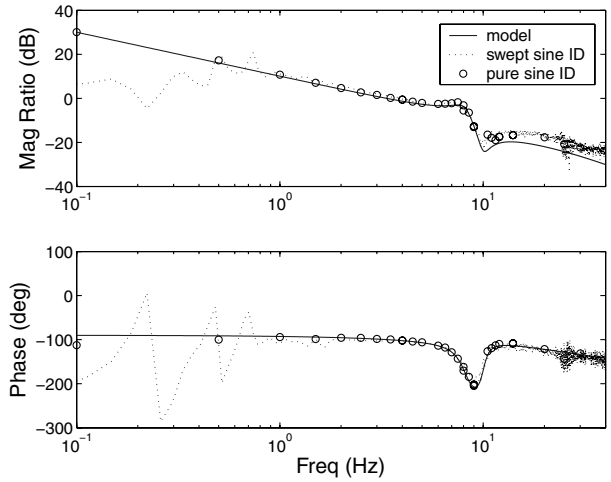

Fig. 2 Comparison of frequency response of the actuator model in (1) to experimental data.

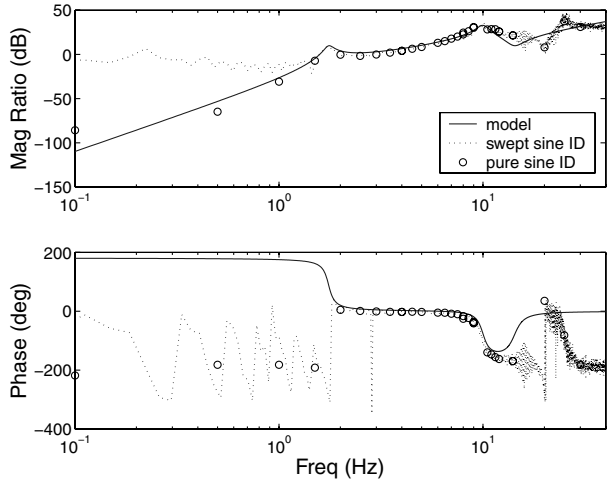

Fig. 3 Comparison of the base acceleration model in (2) to experimental data.

model is presented in [30]). The transfer function for the base acceleration with the joint angle θ as input is given in [29] as

$$\frac{\ddot{x}}{\theta} = P_f(s) = \frac{s^4 B_1}{(s/\omega_1)^2 + 2\zeta_1(s/\omega_1) + 1} + \frac{s^4 B_2}{(s/\omega_2)^2 + 2\zeta_2(s/\omega_2) + 1} \tag{2}$$

where x represents the displacement of the point on which the accelerometer is mounted (see Fig. 1b), and $B_1 = -1/475,000$, $\omega_1 = 1.75$ Hz, $\zeta_1 = 0.05$, $B_2 = 1/(3 \times 10^6)$. The frequency response of the model in (2) is compared with the experimental data in Fig. 3. Note that the model in (2) is only valid up to a frequency of 20 Hz. This means that the dynamics at high frequency are essentially unknown. Furthermore, having 4 zeros at the origin, the values of B_1 and B_2 in (2) of opposite signs lead to having two zeros in the open right-half plane and renders the acceleration output with the input u nonminimum phase. Physically, this is due to the sensor location which is not collocated with the hydraulic actuator (see also Fig. 1b). The uncertainty in high frequency dynamics together with its nonminimum phase property and unmodeled nonlinearities severely restricts the control gains, and thus renders the design of a high-performance vibration controller a challenging task.

Remark 1. A procedure for a general nonlinear model for this application is detailed in [30]. In this paper, we describe the system dynamics as the transfer functions in (1) and (2) so that it can be seen how controlling the micromanipulator (θ) influences vibrations in the flexible base ($\ddot{x}$). The transfer function, when u and $\ddot{x}$ are viewed as input and output, respectively, is obtained as $(\ddot{x}/u) = P_\theta(s)P_f(s)$. These models are derived by curve fitting to the experimental data in which two flexible modes ($\omega_1 = 1.75$ Hz, $\omega_2 = 10$ Hz) are clearly observed. The main feature of the system given in (1) and (2) is the flexible mode ($\omega_p = 8.5$ Hz) in the actuator model, which does not appear when the joint between the link 1 and the link 2 are assumed rigid and the actuator is a velocity source, that is, $\dot{\theta} = Ku$, as in [26,30]. The interactions characterized by the poles and zeros in (1) and (2) as regards to the closed-loop stability are analyzed using the root locus method in [29]. The term τ is a time constant for the hydraulic valve.

III. Existing Control System and Challenges in Adaptive Augmentation Approach

A. Existing Control System

The existing control system in [29] consists of a position controller combined with an inertial damping controller which is *separately* designed to suppress vibration. In spirit, the control scheme is based on separation of bandwidths, or two time scales, in which the fact that the base vibration is relatively "fast" compared with the robot motion is exploited [28]. The rationale can be understood from the block diagram depicted in Fig. 4. The position controller for the rigid link is a proportional feedback

$$u_r = K_r(\theta_d - \theta) \tag{3}$$

where θ_d is the position command for the link, and $K_r = 1$.

It is desirable that the inertial damping controller provides a damping force proportional to the velocity of the base $\dot{x}$. However, this damping force should be generated as an interaction force between link 2 and the base. Under the assumption that the inertial term is dominant, link 2 should be moved so that $\ddot{\theta}$ is proportional to $\dot{x}$. That is, if the hydraulic actuator is a velocity source $\dot{\theta} = Ku$ (this is approximately true up to 8 Hz as can be seen in Fig. 2), u should be obtained in a way that $\dot{u}$ is proportional to $\dot{x}$. This means that the feedback is proportional feedback of the displacement x.

When acceleration is the output as in (2), the displacement cannot be obtained by double integration due to the accelerometer bias. In this case, the root locus analysis in [29] shows that the controller excites the second mode and leads to instability before meaningful damping is obtained for the first mode. Experiments have shown that the second modal shape exhibits positive $\ddot{x}$ in response to torque that leads to positive $\ddot{\theta}$, whereas the first modal shape exhibits negative $\ddot{x}$ in response to the same torque as reflected in the signs of B_1 and B_2 in (2). That is, proportional acceleration feedback adds damping to the first mode, at the expense of reducing the damping in the second mode. Therefore, to reduce the loop gain at the second mode, in [29] a low-pass filter, $G_f(s)$, is applied to the acceleration signal

$$G_f(s) = \frac{1}{(s/\omega_c)^2 + 2\zeta_c(s/\omega_c) + 1} \tag{4}$$

where $\omega_c = 2$ Hz $= 12.6$ rad/s, $\zeta_c = 0.707$. This leads to the control signal $u_f = K_f G_f(s)\ddot{x}$, where $k_f = -1.435$. The overall control signal u_{ec} becomes

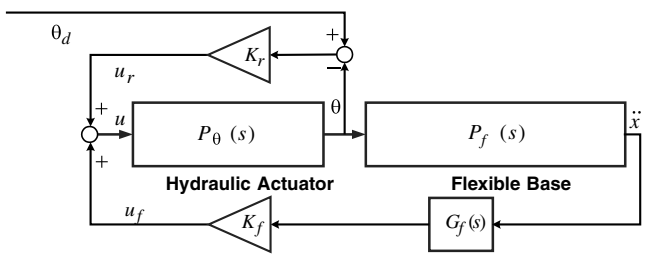

Fig. 4 Existing control system architecture.

$$u_{ec} = u_r + u_f = K_r(\theta_d - \theta) + K_f G_f(s)\ddot{x} \tag{5}$$

as shown in Fig. 4. Further details for the existing controller are given in [29].

B. Challenges in Adaptive Control Augmentation

When attempting to apply the adaptive approach in [43–45] to this system, one immediate difficulty is the lack of control degrees of freedom, that is, a single control input must achieve combined position and vibration control using measurements of joint angle and base vibration. To overcome this problem, a new regulated output variable is defined by blending two outputs

$$\begin{aligned} y_b &= W_1\theta + W_2'\frac{\ddot{x}}{L\omega_1^2} = W_1\theta + W_2\ddot{x} \\ &= \frac{K_1[(s/\omega_2)^2 + 2\zeta_2(s/\omega_2) + 1]}{s(s/\tau + 1)[(s/\omega_p)^2 + 2\zeta_p(s/\omega_p) + 1]} \\ &\times \left\{ W_1 + W_2\left(\frac{s^4 B_1}{(s/\omega_1)^2 + 2\zeta_1(s/\omega_1) + 1} \right.\right. \\ &\left.\left. + \frac{s^4 B_2}{(s/\omega_2)^2 + 2\zeta_2(s/\omega_2) + 1} \right) \right\} u = \frac{P_{b_n}(s)}{P_{b_d}(s)} = P_b(s)u \end{aligned} \tag{6}$$

The weights $W_1 = -0.5$ and $W_2 = 0.1$ were intentionally selected due to the fact that the control has an opposite effect on the base acceleration (moving the link in the positive θ direction leads to negative $\ddot{x}$),

$$\begin{aligned} P_{b_n}(s) = &-(0.3116s^8 + 6.848s^7 + 5038s^6 + 5.716 \times 10^4 s^5 \\ &+ 2.015 \times 10^7 s^4 + 8.885 \times 10^7 s^3 + 2.016 \times 10^{10} s^2 \\ &+ 3.084 \times 10^{10} s + 2.388 \times 10^{12} \end{aligned}$$

and

$$\begin{aligned} P_{b_d}(s) = &\, s^8 + 208.5s^7 + 1.059 \times 10^4 s^6 + 1.362 \times 10^6 s^5 \\ &+ 2.538 \times 10^7 s^4 + 2.161 \times 10^9 s^3 \\ &+ 4.915 \times w0^9 s^2 + 2.388 \times 10^{11} s \end{aligned}$$

It can be seen that when the transfer functions in (1) and (2) are combined, the blended output y_b has relative degree zero. On the other hand, if we introduce the filter in (4) into the blending process following the philosophy of suppressing the high frequency in the measurement in the design of the existing inertial damping controller, the new blended output has relative degree 2

$$\begin{aligned} y_b &= W_1\theta + W_2 G_f(s)\ddot{x} \\ &= \frac{K_1[(s/\omega_2)^2 + 2\zeta_2(s/\omega_2) + 1]}{s(s/\tau + 1)[(s/\omega_p)^2 + 2\zeta_p(s/\omega_p) + 1]} \\ &\times \left\{ W_1 + W_2 \frac{1}{(s/\omega_c)^2 + 2\zeta_c(s/\omega_c) + 1} \right. \\ &\left. \times \left(\frac{s^4 B_1}{(s/\omega_1)^2 + 2\zeta_1(s/\omega_1) + 1} + \frac{s^4 B_2}{(s/\omega_2)^2 + 2\zeta_2(s/\omega_2) + 1} \right) \right\} u \\ &= \frac{P_{bf_n}(s)}{P_{bf_d}(s)} u = P_{bf}(s)u \end{aligned} \tag{7}$$

where

$$\begin{aligned} P_{bf_n}(s) = &-(1317s^8 + 4.411 \times 10^4 s^7 + 1.141 \times 10^7 s^6 \\ &+ 2.801 \times 10^8 s^5 + 2.582 \times 10^{10} s^4 + 4.191 \times 10^{11} s^3 \\ &+ 6.261 \times 10^{12} s^2 + 4.731 \times 10^{13} s + 3.771 \times 10^{14}) \end{aligned}$$

and $P_{bf_d}(s) = (s^2 + 17.769s + 157.914)P_{b_d}(s)$. Because the approach in [43] assumes that the relative degree of the regulated output is greater than zero, the variable y_b in (7) is selected as regulated output variable. In addition, because the electrohydraulic servovalve dynamics lie outside bandwidth of our design (the time constant $\tau = 30$ Hz), y_b is treated as having a practical relative degree of 1 within the bandwidth of our interest. Figure 5 confirms this point by showing that the frequency response of the blended output without the servovalve dynamics has less than 30 deg phase lead and almost identical magnitude response up to 20 Hz compared with the one in (7).

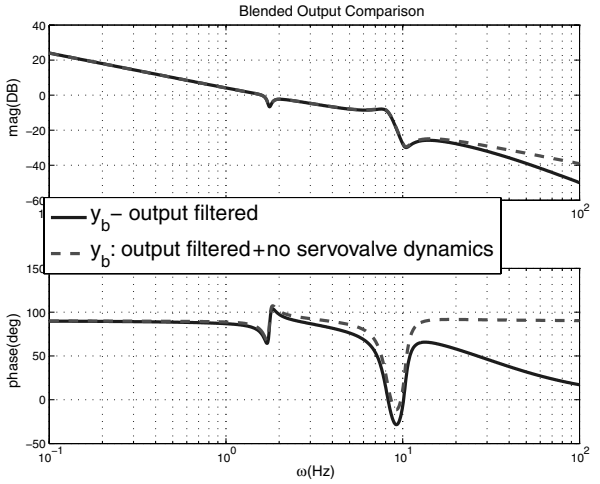

Fig. 5 Comparison of the bounded output in (7) with and without the servovalve dynamics.

Another difficulty in augmenting adaptive elements is associated with constructing a reference model when the existing control system is based on two time scales. In [43–45], adaptive elements are designed in a model following control architecture, and the reference model is defined as the closed-loop dynamics of the plant model being regulated by the existing controller. However, the results in [29] show that the overall performance of the system could be significantly improved if a single coupled controller were designed for the combined dynamics in (1) and (2). Thus the reference model in this application is *designed* as was done in [49] instead of being defined as in [43–45]. A benefit of using the approach in [49] is that it leads to error dynamics that have a lower dimension.

IV. Theoretical Approach

The approach in this paper deviates from those in [43–45] in that: 1) the regulated output is blended using two outputs and 2) a reference model is designed instead of being given as a nominal closed-loop system. As a result of this modification, the regulated output, being still nonminimum phase, is treated as having relative degree one (within the bandwidth of interest). In this section, we address the theoretical aspects of such a modified control scheme and show that a simpler adaptive law for the NN weights than that in [43–45] can be derived. For this, we consider the system described by the following normal form [50]

$$\begin{aligned} \dot{\xi} &= a_1\xi + \boldsymbol{h}_m^T \boldsymbol{z}_1 + bu + \phi_1(\xi, z_1, z_2, u) \\ \dot{\boldsymbol{z}}_1 &= F_m \boldsymbol{z}_1 + \boldsymbol{g}_m \xi + \boldsymbol{\phi}_2(\xi, z_1, z_2), \qquad \dot{z}_2 = \boldsymbol{f}_2(\xi, z_1, z_2) \\ y &= \xi \end{aligned} \tag{8}$$

where $\boldsymbol{z}_1 \in D_{z_1} \subset \mathbb{R}^{m-1}$ is the state of the *modeled* internal dynamics, $z_2 \in D_{z_2} \subset \mathbb{R}^{n-m}$ is the state of unmodeled dynamics, $u \in D_u$ and $y \in D_\xi \subset \mathbb{R}$ are the input and output, respectively, $\phi_1(\xi, z_1, z_2, u)$ is a smooth function and represents a matched uncertainty, and $\boldsymbol{\phi}_2(\xi, z_1, z_2)$ is also assumed smooth and represents an unmatched uncertainty. Notice that the output y has relative degree 1.

Assumption 1. The equilibrium $z_2 = 0$ of $\dot{z}_2 = \boldsymbol{f}_2(0, 0, z_2)$ is globally exponentially stable, the function $\boldsymbol{f}_2(\xi, z_1, z_2)$: $\mathbb{R}^n \to \mathbb{R}^{n-m}$ is globally Lipschitz in its arguments, and $\boldsymbol{\phi}_2$ satisfies the following upper bound:

$$\|\boldsymbol{\phi}_2\| \le \beta_0\|\boldsymbol{x}\| + \beta_1\|z_2\| + \beta_2, \qquad \beta_0, \beta_1, \beta_2 > 0 \tag{9}$$

where $\boldsymbol{x} = [\xi\ z_1^T]^T \in D_x (:= D_\xi \times D_{z_1})$.

Remark 2. From the converse Lyapunov theorem one can deduce that there exists a Lyapunov function $V_{z_2}(z_2)$ satisfying the following conditions [51]:

$$c_1\|z_2\|^2 \le V_{z_2}(z_2) \le c_2\|z_2\|^2, \qquad \frac{\partial V_{z_2}}{\partial z_2}\boldsymbol{f}_2(0,0,z_2) \le -c_3\|z_2\|^2$$
$$\left\|\frac{\partial V_{z_2}}{\partial z_2}\right\| \le c_4\|z_2\| \tag{10}$$

Then, the following upper bound can be derived:

$$\begin{aligned}\dot{V}_{z_2} &= \frac{\partial V_{z_2}}{\partial z_2}\boldsymbol{f}_2(\xi, z_1, z_2)\\ &= \frac{\partial V_{z_2}}{\partial z_2}\boldsymbol{f}_2(0,0,z_2) + \frac{\partial V_{z_2}}{\partial z_2}\boldsymbol{f}_2(\xi, z_1, z_2) - \frac{\partial V_{z_2}}{\partial z_2}\boldsymbol{f}_2(0,0,z_2)\\ &\le -c_3\|z_2\|^2 + c_4c_5\|z_2\|\|\boldsymbol{x}\| \le -\frac{3c_3}{4}\|z_2\|^2 + \frac{(c_4c_5)^2}{c_3}\|\boldsymbol{x}\|^2\end{aligned} \tag{11}$$

where c_5 is the Lipschitz constant of $\boldsymbol{f}_2(\xi, z_1, z_2)$ with respect to $\boldsymbol{x}$. This shows that the $\dot{z}_2 = \boldsymbol{f}_2(\xi, z_1, z_2)$ dynamics, with $\boldsymbol{x}$ as the input, are input-to-state stable [51].

The control architecture in [43–45] is developed by employing a reference model that is the plant model regulated by the existing controller in the absence of uncertainty. With the system in (8), setting $\phi_1 = 0, \boldsymbol{\phi}_2 = 0$, and $z_2 = 0$ leads to a linear model that is used in the design of the existing control system. In practice some control designs may not necessarily involve a linear model, or they may be further tweaked in an operational setting. As a consequence, the reference model derived as the plant model regulated by the implemented existing control system may not necessarily describe the desired closed-loop behavior. In this case, we can *design* a reference model so that it exhibits the desired closed-loop characteristic and apply the method in [43–45]. For the system in (8), we follow this path and design the following state feedback controller,

$$u_{rm} = -k_1\xi_m - \boldsymbol{k}_2^T z_l + k_3 y_d \tag{12}$$

and derive a reference model having the form

$$\dot{\boldsymbol{x}}_m = \bar{A}\boldsymbol{x}_m + \bar{\boldsymbol{b}}k_3 y_d, \qquad \boldsymbol{x}_m(0) = 0, \qquad y_l = \bar{\boldsymbol{c}}^T\boldsymbol{x}_m \tag{13}$$

where $\boldsymbol{x}_m = [\xi_m \quad \boldsymbol{z}_m^T]^T \in \mathbb{R}^m$, and

$$\bar{A} = \begin{bmatrix} a_1 - bk_1 & \boldsymbol{h}_m^T - b\boldsymbol{k}_2^T \\ \boldsymbol{g}_m & F_m \end{bmatrix}, \qquad \bar{\boldsymbol{b}} = \begin{bmatrix} b \\ 0 \end{bmatrix}_{m\times 1}$$
$$\bar{\boldsymbol{c}} = \begin{bmatrix} 1 \\ 0 \end{bmatrix}_{m\times 1} \tag{14}$$

The subscript m is used for the states of the reference model, and y_d is a *bounded* reference command, that is, $\|y_d(t)\| \le \beta_c$ for $t \ge 0$. Given $\bar{A}$ Hurwitz and a bound for y_d, it follows that there exists a $\beta_3 > 0$ such that

$$\|\boldsymbol{x}_m(t)\| \le \beta_3, \quad \forall\ t \ge 0 \tag{15}$$

Let

$$u = u_{ec} + u_{ad} \tag{16}$$

where u_{ec} is the output of the existing controller, and u_{ad} is the control signal used to compensate for uncertainty. Define the error vector

$$\boldsymbol{E} = \begin{bmatrix} \xi_m - \xi \\ z_m - z_1 \end{bmatrix} = \begin{bmatrix} e \\ \tilde{z}_1 \end{bmatrix}, \qquad \boldsymbol{E} \in \mathbb{R}^m \tag{17}$$

Comparing (8) to (13) leads to the following expression for the *error dynamics*:

$$\dot{\boldsymbol{E}} = \bar{A}\boldsymbol{E} + \bar{\boldsymbol{b}}(-u_{ad} - \Delta_1) - B_2\boldsymbol{\phi}_2, \qquad \dot{z}_2 = \boldsymbol{f}_2(\xi, z_1, z_2)$$
$$e = \bar{\boldsymbol{c}}^T\boldsymbol{E} \tag{18}$$

where

$$B_2 = \begin{bmatrix} 0 \\ I_{(m-1)\times(m-1)} \end{bmatrix},$$
$$\Delta_1 = (1/b)\phi_1(\xi, z_1, z_2, u) + k_1\xi + \boldsymbol{k}_2^T z_1 - k_3 y_d + u_{ec} \tag{19}$$

Let

$$u_{ad} = -u_{nn} - u_{dc} \tag{20}$$

where u_{nn} is the output of the NN to approximately cancel Δ_1, and u_{dc} is the output of the following linear controller:

$$\dot{\boldsymbol{x}}_{dc} = A_{dc}\boldsymbol{x}_{dc} + \boldsymbol{b}_{dc}e, \quad \boldsymbol{x}_{dc} \in \mathbb{R}^{n_{dc}} \quad u_{dc} = \boldsymbol{c}_{dc}^T\boldsymbol{x}_{dc} + d_{dc}e \tag{21}$$

This additional control signal is introduced to robustify the adaptation process, and reduce the error bounds in the stability analysis [43]. Applying the controller in (21) to the dynamics in (18) leads to the following augmented error dynamics:

$$\dot{\boldsymbol{E}}_a = F\boldsymbol{E}_a + \begin{bmatrix} \bar{\boldsymbol{b}} \\ 0 \end{bmatrix}(u_{nn} - \Delta_1) - \begin{bmatrix} B_2 \\ 0 \end{bmatrix}\boldsymbol{\phi}_2 \quad \dot{z}_2 = \boldsymbol{f}_2(\xi, z_1, z_2) \tag{22}$$

where

$$\boldsymbol{E}_a = \begin{bmatrix} \boldsymbol{E} \\ \boldsymbol{x}_{dc} \end{bmatrix} \in \mathbb{R}^{m+n_{dc}}, \qquad F = \begin{bmatrix} \bar{A} + \bar{\boldsymbol{b}}d_{dc}\bar{\boldsymbol{c}}^T & \bar{\boldsymbol{b}}\boldsymbol{c}_{dc}^T \\ \boldsymbol{b}_{dc}\bar{\boldsymbol{c}}^T & A_{dc} \end{bmatrix} \tag{23}$$

Because F is Hurwitz by design, there exist a $P = P^T > 0$ such that, for any $Q > 0$,

$$F^TP + PF + Q = 0 \tag{24}$$

Notice from (16) and (20) that Δ_1 in (19) depends on u_{nn} through u, and that the role of u_{nn} is to cancel Δ_1. This constitutes a fixed point problem.

Assumption 2. The mapping $u_{nn} \mapsto \Delta_1(\boldsymbol{x}, z_2, u)$ is a contraction uniformly in $(\boldsymbol{x}, z_2) \in D_x \times D_{z_2}$ on D_u.

Following the analysis in [40], we can derive sufficient conditions for Assumption 2. Using (19), Assumption 2 implies that there exists a $\rho > 0$ such that:

$$\left|\frac{\partial\Delta_1(\boldsymbol{x}, z_2, u)}{\partial u_{nn}}\right| = \left|\frac{1}{b}\left(\frac{\partial\dot{\xi}}{\partial u} - b\right)\right| = \left|\frac{\partial\dot{\xi}}{\partial u}\Big/ b - 1\right| \le \rho < 1 \tag{25}$$

which is guaranteed by the following conditions:

$$\operatorname{sgn}(b) = \operatorname{sgn}\left(\frac{\partial\dot{\xi}}{\partial u}\right) \qquad \left|\frac{\partial\dot{\xi}}{\partial u}\right|\Big/ 2 < |b| < \infty \tag{26}$$

These conditions mean that control reversal is not permitted and there is a lower bound on the estimate of the control effectiveness term b.

A single hidden layer, multiperceptron NN is used to approximate Δ_1 in (19). Because it is a function of states and control, we recall the main result from [52] which establishes a universal approximation for an unknown function of the states and control in an *observable* system using sampled values of its input/output.

Theorem 1. For arbitrary $\epsilon^* > 0$, there exist bounded constant weights M, N such that:

$$\Delta_1(\boldsymbol{x}, z_2, u) = M^T\boldsymbol{\sigma}(N^T\boldsymbol{\eta}) + \varepsilon(\boldsymbol{\eta}), \qquad \|\varepsilon(\boldsymbol{\eta})\| \le \epsilon^*$$
$$(\boldsymbol{x}, z_2, u) \in D_x \times D_{z_2} \times D_u \tag{27}$$

where $\varepsilon(\boldsymbol{\eta})$ is the NN reconstruction error and $\boldsymbol{\eta}$ is the network input vector

$$\begin{aligned}\boldsymbol{\eta}(t) &= \left[1 \;\; y_d(t) \;\; u_{ec}(t) \;\; \bar{\boldsymbol{u}}_d^T(t) \;\; \bar{\boldsymbol{y}}_d^T(t)\right]^T \in \mathbb{R}^{n_\eta}, \qquad \|\boldsymbol{\eta}\| \le \eta^* \\ \bar{\boldsymbol{u}}_d^T(t) &= [u(t) \;\; u(t-d) \;\; \cdots u(t-(n_1-r-1)d)]^T \\ \bar{\boldsymbol{y}}_d^T(t) &= [y(t) \;\; y(t-d) \;\; \cdots y(t-(n_1-1)d)]^T \end{aligned} \tag{28}$$

in which n_1 is the length of the window and generally required to be greater or equal to the system dimension n, $d > 0$ is a time delay, r is the relative degree of the output, $\boldsymbol{\sigma} \in \mathbb{R}^{n_\sigma+1}$ is a vector of squashing functions ([34], p. 55), in which $\sigma_1 = 1$, and its ith element is defined as $[\boldsymbol{\sigma}(N^T\boldsymbol{\eta})]_i = \sigma[(N^T\boldsymbol{\eta})_i]$ for $2 \le i \le n_\sigma + 1$.

The adaptive signal u_{nn} is expressed in the form

$$u_{nn} = \hat{M}^T\boldsymbol{\sigma}(\hat{N}^T\boldsymbol{\eta}) \tag{29}$$

where $\hat{M}$ and $\hat{N}$ are weights that are adapted by the following update law:

$$\begin{aligned}\dot{\hat{M}} &= -\Gamma_M[(\hat{\boldsymbol{\sigma}} - \hat{\sigma}'\hat{N}^T\boldsymbol{\eta})e p_{11} b + k\hat{M}], \\ \dot{\hat{N}} &= -\Gamma_N[e p_{11} b\boldsymbol{\eta}\hat{M}^T\hat{\sigma}' + k\hat{N}]\end{aligned} \tag{30}$$

in which Γ_M, $\Gamma_N > 0$ are positive definite adaptation gain matrices, $k > 0$ is a σ-modification constant, $\hat{\boldsymbol{\sigma}} \triangleq \boldsymbol{\sigma}(\hat{N}\boldsymbol{\eta})$, $\hat{\sigma}'$ is the Jacobian computed at the estimates, and p_{11} is obtained from the decomposition of P in (24) as follows:

$$P = \begin{bmatrix} p_{11} & \boldsymbol{p}_{21}^T \\ \boldsymbol{p}_{21} & P_{22}\end{bmatrix} p_{11} \in \mathbb{R}, \qquad \boldsymbol{p}_{21} \in \mathbb{R}^{n_{dc}+m-1} \tag{31}$$

Notice that unlike [43], the adaptive law in (30) does not require an error observer for the teaching signal for the NN. This is due to the fact that the system output has relative degree 1 and only the portion of the positive matrix P is used in the adaptive law.

Define

$$\tilde{M} \triangleq \hat{M} - M, \qquad \tilde{N} \triangleq \hat{N} - N, \qquad \tilde{Z} \triangleq \begin{bmatrix} \tilde{M} & 0 \\ 0 & \tilde{N}\end{bmatrix} \tag{32}$$

where M, N are ideal weights defined in (27). The stability proof will establish ultimate boundedness ([51], p. 211) of all the closed-loop signals by showing that the signals $\boldsymbol{z}_2$ and $\boldsymbol{E}_a$ in (22) and the NN weight errors $\tilde{Z}$ in (32) are bounded. With this objective in mind, we define the vector $\boldsymbol{\zeta} \triangleq [\boldsymbol{E}_a^T \; \boldsymbol{z}_2^T \; \mathrm{vec}(\tilde{Z})^T]^T$, where the operator vec is stacking a matrix into a vector, and a hypersphere in the error space:

$$B_R \triangleq \{\boldsymbol{\zeta} | \|\boldsymbol{\zeta}\| \le R\}, \qquad R > 0 \tag{33}$$

such that for every $\boldsymbol{\zeta} \in B_R$, we have $(\boldsymbol{x}, \boldsymbol{z}_2, u) \in D_x \times D_{z_2} \times D_u$.

Consider the following Lyapunov candidate function:

$$\begin{aligned}V(\boldsymbol{E}_a, \boldsymbol{z}_2, \tilde{M}, \tilde{N}) &= \boldsymbol{E}_a^T P \boldsymbol{E}_a + \tfrac{1}{2}\tilde{M}^T\Gamma_M^{-1}\tilde{M} \\ &\quad + \tfrac{1}{2}\mathrm{tr}(\tilde{N}^T\Gamma_N^{-1}\tilde{N}) + V_{z_2}\end{aligned} \tag{34}$$

With the following gain matrices

$$\begin{aligned}T_1 &= \frac{1}{2}\begin{bmatrix} 2P & 0 & 0 & 0 \\ 0 & \Gamma_M^{-1} & 0 & 0 \\ 0 & 0 & \Pi_N^{-1} & 0 \\ 0 & 0 & 0 & 2c_1 I\end{bmatrix}, \\ T_2 &= \frac{1}{2}\begin{bmatrix} 2P & 0 & 0 & 0 \\ 0 & \Gamma_M^{-1} & 0 & 0 \\ 0 & 0 & \Pi_N^{-1} & 0 \\ 0 & 0 & 0 & 2c_2 I\end{bmatrix}\end{aligned} \tag{35}$$

where I is the identity matrix of dimension $(n-m)\times(n-m)$, and

$$\Pi_N = \begin{bmatrix} \Gamma_N & 0 & \dots & 0 \\ 0 & \Gamma_N & \dots & 0 \\ \vdots & \vdots & \ddots & \vdots \\ 0 & 0 & \dots & \Gamma_N\end{bmatrix}_{n_\sigma n_\eta \times n_\sigma n_\eta} \tag{36}$$

the following inequality is immediate from (10)

$$\boldsymbol{\zeta}^\top T_1 \boldsymbol{\zeta} \le V(\boldsymbol{\zeta}) \le \boldsymbol{\zeta}^\top T_2 \boldsymbol{\zeta} \tag{37}$$

Let

$$\alpha_M \triangleq \min_{\|\boldsymbol{\zeta}\|=R} \boldsymbol{\zeta}^\top T_1 \boldsymbol{\zeta} = R^2 T_{1_m}$$

where T_{1_m} is the minimum eigenvalue of T_1. Introduce the following set:

$$\Omega_{\alpha_M} = \{\boldsymbol{\zeta} \in B_R | \boldsymbol{\zeta}^\top T_1 \boldsymbol{\zeta} \le \alpha_M\} \tag{38}$$

Assumption 3. Assume

$$R > \gamma\sqrt{\frac{T_{2_M}}{T_{1_m}}} \ge \gamma \tag{39}$$

where T_{2_M} is the maximum eigenvalue of the matrix T_2 in (35), and γ is defined in (A20).

Theorem 2. Let Assumptions 1–3 hold. Then, if the initial error $\boldsymbol{\zeta}(0)$ belongs to the compact set Ω_{α_M} in (38), the feedback control law given by (16) and (20), along with (21) and (30), guarantees that the signals $\boldsymbol{E}_a$, $\boldsymbol{z}_2$, $\tilde{Z}$ in the closed-loop system are uniformly ultimately bounded provided that the conditions in (A6) and (A8) are satisfied.

Proof. See the Appendix.

Remark 3. Assumption 3 may be interpreted as implying both an upper and lower bound for the adaptation gains. Define $\bar{\gamma} \triangleq \max(\lambda_{\max}(\Gamma_M), \lambda_{\max}(\Gamma_N))$, $\underline{\gamma} \triangleq \min(\lambda_{\min}(\Gamma_M), \lambda_{\min}(\Gamma_N))$ and $\bar{\lambda} \triangleq \max(\lambda_{\max}(P), c_2)$ and $\underline{\lambda} \triangleq \min(\lambda_{\min}(P), c_1)$, where $\lambda(\cdot)$ denotes the eigenvalue. Then an upper bound for the adaptation gains results when $2\bar{\lambda}\,\underline{\gamma} > 1$ and $2\underline{\lambda}\,\bar{\gamma} > 1$, for which the relation in (39) reduces to $\bar{\gamma} < R^2/(2\gamma^2\bar{\lambda})$. A lower bound for the adaptation gains results when $2\bar{\lambda}\,\underline{\gamma} < 1$ and $2\underline{\lambda}\,\bar{\gamma} < 1$, for which (39) reduces to $\underline{\gamma} > \gamma^2/(2R^2\underline{\lambda})$.

Remark 4. In contrast to the approaches in [43–45], the approach adopted here permits us to treat the design as having relative degree one (within the bandwidth of interest). Consequently, we do not require an estimate of the derivative of the tracking error. Otherwise, the approach shares the same assumptions as in [43–45] and has the same restrictions on the unmodeled dynamics. In addition, although the approach in this section is formulated in a single-input single-output setting, the approach can also be extended to a multi-input multi-output systems following the formulation given in [44].

V. Adaptive Control Implementation

A. Reference Model Design

In the design of a reference model, we consider only the first flexible mode in the base from the system in (2)

$$\frac{\ddot{x}_m}{\theta_m} = \frac{s^4 B_1}{(s/\omega_1)^2 + 2\zeta_1(s/\omega_1) + 1} \tag{40}$$

and a simplified hydraulic actuator model

$$\frac{\theta_m}{u} = \frac{K_1}{s[(s/\omega_p)^2 + 2\zeta_p(s/\omega_p) + 1]} \tag{41}$$

This model ignores the electrohydraulic servovalve dynamics and its high frequency zero. Although the blended output in (7) involves the low-pass filter in (4) due to the second mode, the system in (40) and (41) does not consider the second mode. Therefore, the output of the reference model is defined without the low-pass filter

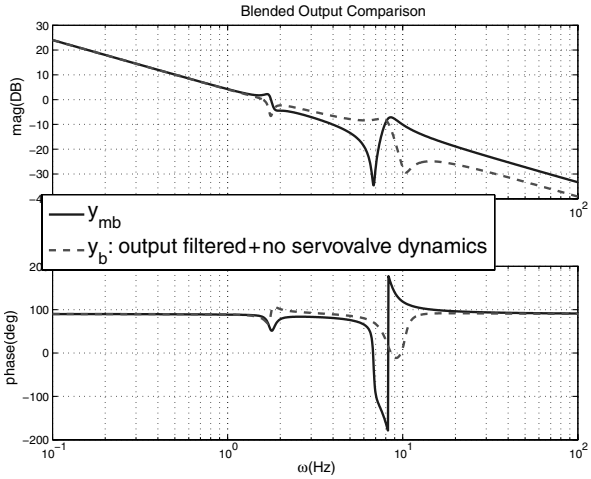

Fig. 6 Comparison of the blended output of the design model to that in (7) without servovalve dynamics.

$$\begin{aligned} y_{m_b} &= W_1\theta_m + W_2\ddot{x}_m \\ &= \frac{K_1}{s[(s/\omega_p)^2 + 2\zeta_p(s/\omega_p) + 1]}\frac{s^4 B_1}{(s/\omega_1)^2 + 2\zeta_1(s/\omega_1) + 1}u \\ &= P_{mb}(s)u \end{aligned} \tag{42}$$

which has relative degree 1 that is the same as that in (7) without the servovalve dynamics, as shown in Fig. 6. In this figure, the frequency response of the blended output in (42) is compared with that in (7) assuming the effect of electrohydraulic servovalve dynamics are not present. The blended output in (42) is described in the following state space form:

$$\dot{\boldsymbol{\chi}} = A_m\boldsymbol{\chi} + \boldsymbol{b}_m u, \qquad y_{m_b} = \boldsymbol{c}_m^T\boldsymbol{\chi} \tag{43}$$

where

$$A_m = \begin{bmatrix} -10.3044 & -41.4770 & 0 & 0 & 0 \\ 64 & 0 & 0 & 0 & 0 \\ 0 & 8.0 & 0 & 0 & 0 \\ 12.9616 & 0 & 0 & -1.0996 & -7.5564 \\ 0 & 0 & 0 & 16.0 & 0 \end{bmatrix}$$

$$\boldsymbol{b}_m = \begin{bmatrix} 16 \\ 0 \\ 0 \\ 0 \\ 0 \end{bmatrix}, \qquad \boldsymbol{c}_m = \begin{bmatrix} -0.8446 \\ 0 \\ -3.2404 \\ 0.0716 \\ 0.4924 \end{bmatrix} \tag{44}$$

As a next step, we design a linear quadratic regulator (LQR) controller for the design model in (43) which minimizes the cost integral

$$J = \int_0^\infty (\boldsymbol{\chi}^T Q_\chi \boldsymbol{\chi} + Ru^2)\,\mathrm{d}x \tag{45}$$

where $Q_\chi = \mathrm{diag}\{0.5, 0.5, 0.5, 1.5, 2.5\}$ and $R = 0.01$. The resulting controller is as follows:

$$u_{\mathrm{lqr}} = -K_{\mathrm{lqr}}(\boldsymbol{\chi} - \boldsymbol{\chi}_d) \tag{46}$$

where $\boldsymbol{\chi}_d = [\,\theta_d \quad 0 \quad 0 \quad 0 \quad 0\,]^T$ represents the steady state vector which generates the desired position angle θ_d for the link, and $K_{\mathrm{lqr}} = [\,9.7192 \quad 8.1810 \quad 7.0711 \quad -5.2252 \quad 13.5296\,]$.

Following the procedure in ([51], pp. 531–545) that leads to the following transformation matrix:

$$T_m = \begin{bmatrix} -0.8446 & 0 & -3.2404 & 0.0716 & 0.4924 \\ 0 & 0 & 0 & -1.0426 & 0 \\ 0 & 0 & 0 & 0 & -2.0851 \\ 0 & -0.4471 & 0 & 2.2075 & 0.1517 \\ 0 & 0.0651 & -0.8942 & -0.3212 & 2.1855 \end{bmatrix} \tag{47}$$

the system in (43) can be transformed into the following normal form:

$$\dot{\boldsymbol{\chi}}_m = A'_m\boldsymbol{\chi}_m + \boldsymbol{b}'_m u, \qquad y_{m_b} = \boldsymbol{c}'^T_m\boldsymbol{\chi}_m \tag{48}$$

where $\boldsymbol{\chi}_m = T_m\boldsymbol{\chi}$, $A'_m = T_m A_m T_m^{-1}$, $\boldsymbol{b}'_m = T_m\boldsymbol{b}_m$, $\boldsymbol{c}'^T_m = \boldsymbol{c}_m^T T_m^{-1}$. Letting $\boldsymbol{\chi}_m = [\xi_m, \boldsymbol{z}_m^T]^T$ leads for the system in (48) to be written in the decomposed form in (8)

$$\begin{gathered} \dot{\xi}_m = a_1\xi_m + +\boldsymbol{h}_m^T\boldsymbol{z}_m + bu \qquad \dot{\boldsymbol{z}}_m = F_m\boldsymbol{z}_m + \boldsymbol{g}_m\xi_m \\ y_{m_b} = \xi_m \end{gathered} \tag{49}$$

where $\xi_m \in \mathbb{R}$, $\boldsymbol{z}_m \in \mathbb{R}^4$, $a_1 = -11.404$, $b = -13.5132$, and

$$\boldsymbol{h}_m = \begin{bmatrix} -51.3982 \\ 39.8383 \\ -14.3573 \\ 41.3276 \end{bmatrix},$$

$$F_m = \begin{bmatrix} 0 & -61.3872 & -8.4373 & -57.9834 \\ 32 & 0 & 0 & 0 \\ 0 & 8 & 0 & 0 \\ 0 & 0 & 16 & 0 \end{bmatrix}, \tag{50}$$

$$\boldsymbol{g}_m = \begin{bmatrix} 16 \\ 0 \\ 0 \\ 0 \end{bmatrix}$$

Using the transformation in (47), the LQR controller in (46) can be expressed as

$$u_{\mathrm{lqr}} = -K_{\mathrm{lqr}}T_m^{-1}(\boldsymbol{\chi}_m - \boldsymbol{\chi}_{m_d}) = -k_1\xi_m - \boldsymbol{k}_2^T\boldsymbol{z}_m + k_1\theta_d \tag{51}$$

where $\boldsymbol{\chi}_{m_d} = T_m\boldsymbol{\chi}_d$, $k_1 = -11.5078$, $\boldsymbol{k}_2^T = [-34.5251, 25.2423, -13.3812, 33.7958]$. The design model in (49) regulated by the controller in (51) leads to the reference model in (13).

The performance of the reference model is compared with that of the combined model of (1) and (2) regulated by the existing controller of (3) and (4) in Fig. 7 for a reference command corresponding to the step response of the following command filter

$$P_d(s) = \frac{1}{(s/\omega_d)^2 + 2\zeta_d(s/\omega_d) + 1} \tag{52}$$

where $w_d = 10$ rad/s, $\zeta_d = 0.8$.

The reference model achieves less oscillatory tracking response in the position control of the link with much less vibration in the base compared with the closed loop of the combined model of (1) and (2) under the regulation of the existing controller. Thus use of this reference model in the adaptive design implies that the adaptive controller aims to achieve a higher level of performance in the presence of modeling error than that of the existing controller in the absence of modeling error. The performance of the adaptive controller depends on how close the adaptive signal u_{nn} approximates the matched uncertainty $\Delta_1(\boldsymbol{x}, z_2, u)$ and the size of the unmatched uncertainty $\boldsymbol{\phi}_2(\boldsymbol{x}, z_2)$ characterized by (9).

B. Augmenting Adaptive Elements

The controller in (21) is designed as a lead compensator,

$$u_{dc} = 0.2\frac{s/3 + 1}{s/20 + 1}e \tag{53}$$

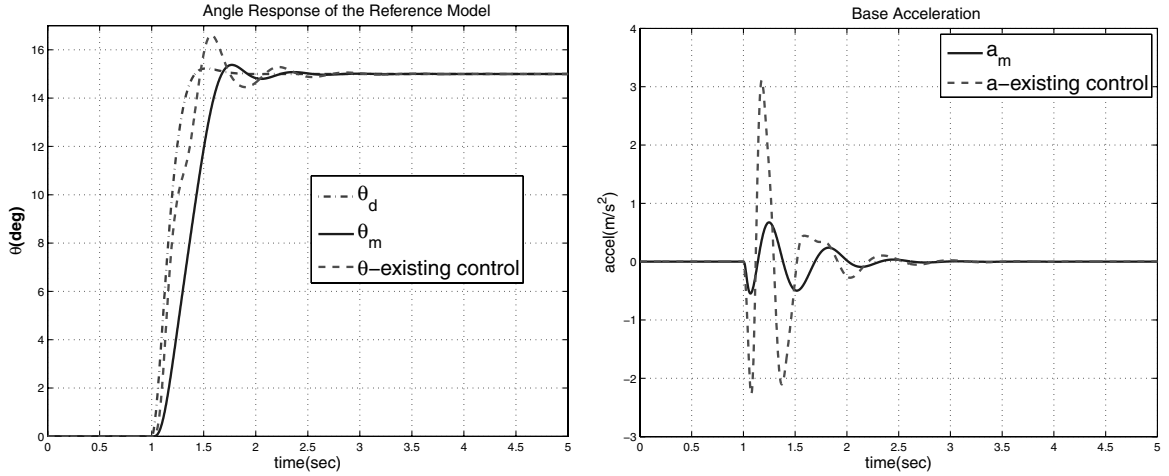

a) Response of the joint angle **b) Response of the base acceleration**

Fig. 7 Comparison of responses between the reference model and the combined model of (1) and (2) regulated by the existing controller.

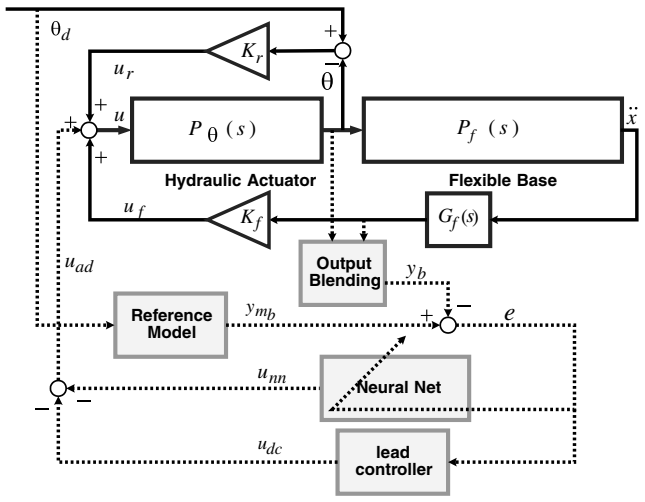

Fig. 8 Adaptive control augmenting architecture.

For Assumption 2, the conditions in (26) are easily checked using (7) and (49) which directly provides the gains $(\partial\dot{\xi}/\partial u) = -1378/\tau = -7.31$ and $b = -13.5132$ if we treat the hydraulic servovalve dynamics outside the bandwidths of interest. This is valid up to 20 Hz as shown in Fig. 5. This can also be deduced by investigating the frequency responses in Fig. 6. According to ([51], p. 538), in the case of a transfer function for a single-input/single-output linear time-invariant system, the control effectiveness term is derived as the first coefficient of the nominator polynomial when the denominator is a monic polynomial. Therefore, $(y_{m_b}/u)(s) \approx (b/s)$ when $s = j\infty$. Figure 6 shows that y_b/u and y_{m_b}/u have the same roll-off slope (=1), the same phase, and $|P_{bf}(j\omega)| < |P_{mb}(j\omega)|$ when $\omega = \infty$. This ensures that the conditions in (26) are met. To circumvent a fixed point iteration in the real-time environment, the control signal is delayed by the single sampling time before it is used as a network input. In a preliminary simulation, this was compared with obtaining a fixed point solution, and the results were indistinguishable.

The NN consists of seven neurons in the hidden layer ($n_\sigma = 6$). Because the system dimension is not exactly known, nine delayed values of y_b in (7) and eight delayed values of the input u, with delay $d = 0.02$ s, are combined to construct the NN input signal. The squashing functions are chosen as sigmoidal functions

$$[\boldsymbol{\sigma}(N^T\boldsymbol{\eta})]_i = \frac{1}{1 + e^{-a(N^T\boldsymbol{\eta})_i}}, \qquad i = 2, \ldots, 7 \tag{54}$$

where $a = 1$ represents the activation potential. The Lyapunov equation in (24) is solved by setting $Q = 1.1I_{6\times6}$. The following parameters are used for the adaptive law in (30):

$$\Gamma_M = 0.05I_{7\times7}, \qquad \Gamma_N = 0.06I_{20\times20}, \qquad k = 0.1 \tag{55}$$

The overall NN-based adaptive control architecture is depicted in Fig. 8, where the elements used to augment the existing control system are shaded.

VI. Experimental Results

To analyze the effectiveness of the existing control scheme and the NN-based augmenting scheme during two-dimensional robot motion, a square wave of magnitude 15 deg and frequency of 0.025 Hz is applied through the command filter in (52) with all other degrees of freedom locked. The control objective is to achieve inertial tip positioning of the end effector attached to the micromanipulator. Relative rotation of the joint angle with respect to the base θ is measured by an encoder, and the base acceleration $\ddot{x}$ is measured by an accelerometer (see Fig. 1b).

The joint angle θ and the base acceleration $\ddot{x}$ responses are shown in Fig. 9. Dashed lines represent the responses without the inertial damping controller ["without u_f," that is, $u = u_r$ in (3)], dotted lines represent the responses with the inertial damping controller ["u_f without u_{ad}," that is, $u = u_{ec}$ in (5)], and the solid lines represent the responses with adaptive augmentation ["u_f with u_{ad}," that is, $u = u_{ec} + u_{ad}$ in (16)]. Because of the scale used in these figures, the differences in responses are hard to distinguish, but selected regions are zoomed in successive figures below.

Figure 10 shows the differences in transient response for each of the different control strategies. Without damping control, the joint angle tracks the reference command very closely, but the base acceleration is completely uncontrolled. This results in a long settling time because of the long vibration decay time. In contrast, with the inertial damping control added ("u_f without u_{ad}"), the responses in Figs. 10a and 10b show that the micromanipulator is moved by the controller in a manner to damp the base vibration. At the expense of a slight overshoot with oscillations in the joint angle, the acceleration in the flexible base is greatly diminished. The frequency content observed in the joint angle shows that the first mode vibration is damped. When adaptive augmentation is applied ("u_f with u_{ad}"), similar transient responses with the inertial damping controller are observed. However, the joint angle response exhibits the movement of the micromanipulator before it is moved into place in contrast to the inertial damping controller that moves the joint and then damps the vibration. As a result, settling time has increased slightly.

Inspection of the steady state responses from Fig. 9 as shown in Fig. 11 reveals interesting features of the different controllers. With

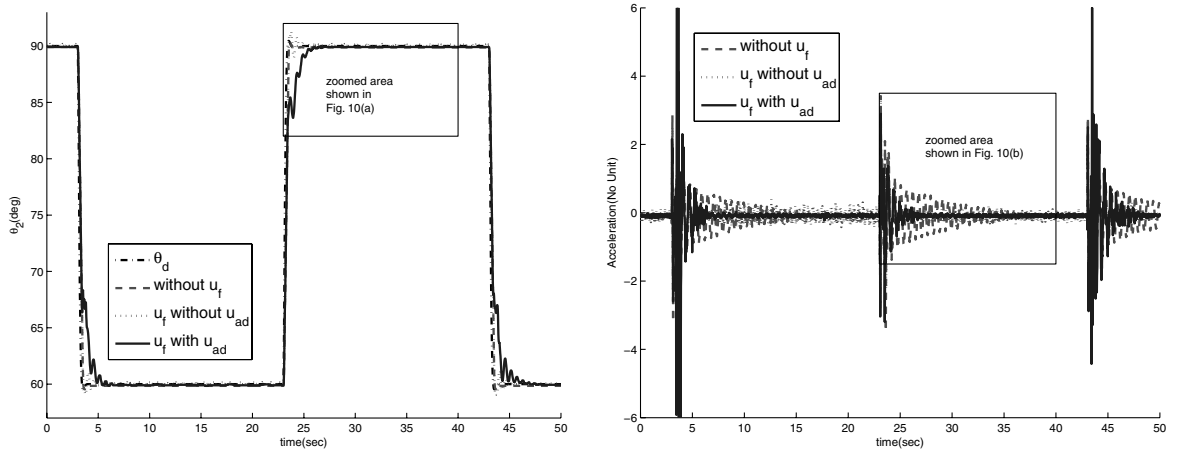

a) b)

Fig. 9 Comparison of output responses a) of the joint angle and b) of the base acceleration, with a square wave reference command.

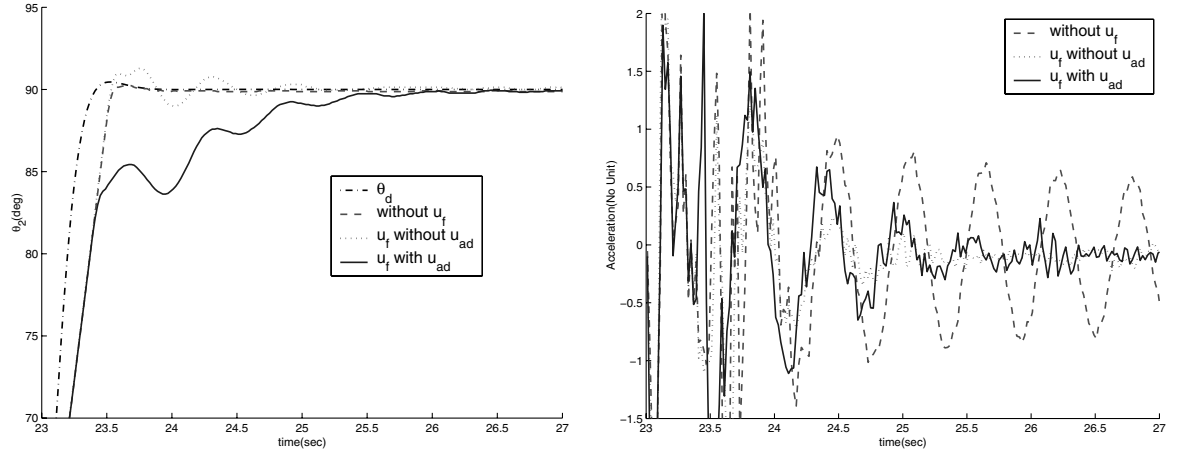

a) b)

Fig. 10 Comparison of transient responses a) of the joint angle and b) of the base acceleration.

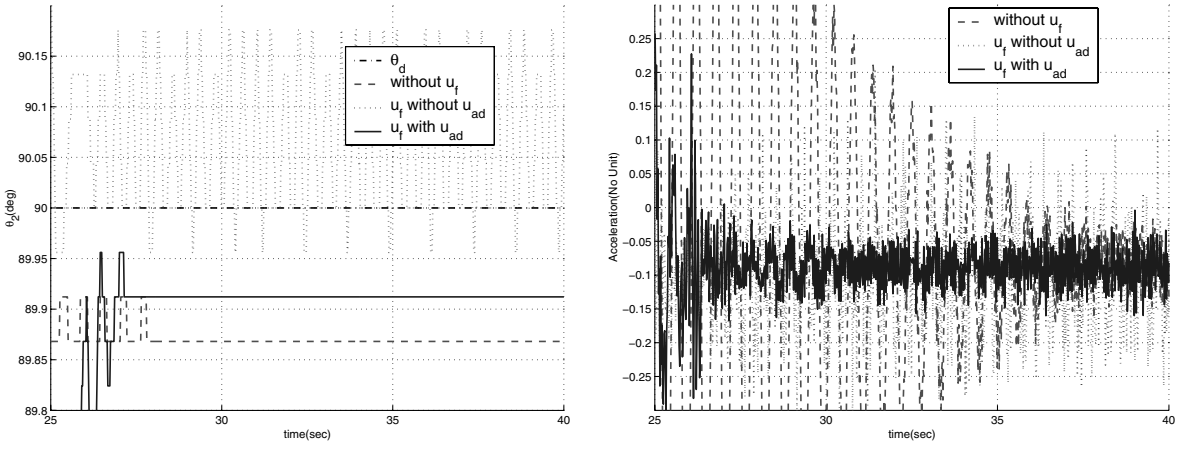

a) b)

Fig. 11 Comparison of steady state responses a) of the joint angle and b) of the base acceleration.

the existing control system, the joint angle oscillates around a value that is offset from the desired angle due to actuator nonlinearities such as dead zone and stiction. The nonlinearities in the actuation are configuration dependent and time varying, depending on operating conditions. This implies that the fixed gain control deviates when it encounters an uncertain operating condition. This behavior is problematic if the manipulator is to be employed for tasks requiring high precision. In contrast, the augmented control regulates the joint

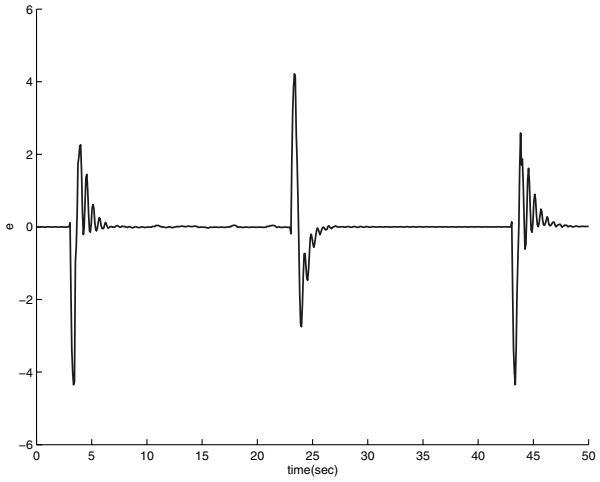

Fig. 12 The tracking error e in (17).

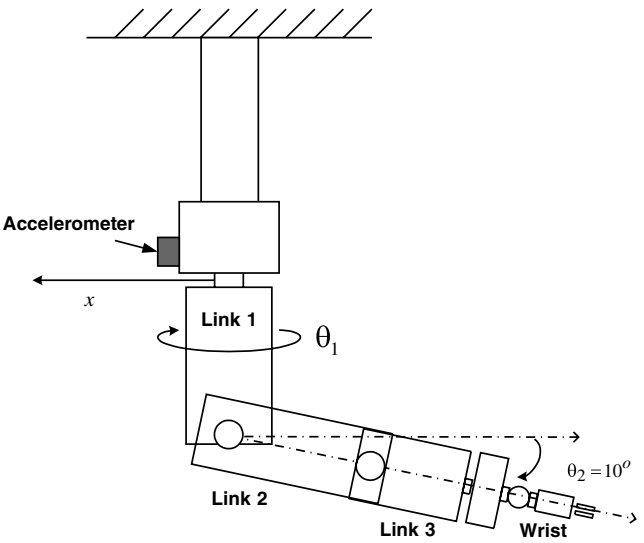

Fig. 14 Configuration with $\theta_1 = -90$ deg, $\theta_2 = 10$ deg, $\theta_3 = 0$ deg, and $x = 0$.

angle close to the accuracy of the encoder resolution (0.044 deg), and it suppresses the vibration to that level without damping control (without damping control, the vibration decays completely to zero in its steady state response, thus oscillations in the acceleration measurement are due to sensor noise). The action of the adaptive elements in augmenting the existing control can be explained by investigating the tracking error e in (17). This error is the deviation of the regulated output from that of the reference model, and Fig. 12 shows this error. With the adaptive control, the error is regulated close to zero. This is only possible when the regulation of the joint angle and the suppression of the base vibration are achieved simultaneously, because the regulated output combines the joint angle and the base vibration.

To illustrate the potential benefits of the augmenting adaptive controller in improving robustness, additional lead weights are mounted on the wrist in Fig. 1 to test the performance of the different controllers when the inertia property changes. This mass change simulates the situation when the manipulator picks up a massive object and alters the frequencies of the flexible modes. For example, adding approximately 6.35 kg leads to the frequency change of the first mode from 1.75 Hz to 1.55 Hz. In this case, the existing controller in (5) suppresses the first mode vibration, but excites the second mode and results in an instability. The augmented controller effectively damps out the vibration and achieves fine tip positioning in the joint angle. A further increase in the inertia by adding more lead weights (approximately 10.56 kg) leads to the time responses shown in Fig. 13. Without the augmenting elements, the existing system immediately goes unstable whereas the augmented control system quickly stabilizes the unstable system and maintains good performance. This demonstrates robustness of the adaptive approach to mass variations at the tip of the manipulator.

Finally, to further illustrate the augmented controller, the test is also performed with the configuration in Fig. 14, which is described by $\theta_1 = -90$ deg, $\theta_2 = 10$ deg, $\theta_3 = 0$ deg, and $x = 0$ according to the definitions given in Fig. 1b. Because the linear models in (1) and (2) are derived based on the experimental data with the configuration in Fig. 1a, it is not valid with the configuration in Fig. 14. The experiment is carried out by pushing the base which mimics an impulsive type of external disturbance and switching the adaptive control on and off to observe how the control systems behave in Fig. 15. Because the configuration belongs to a region in which the linear model is not valid, the existing inertial damping control system leads to instability when the base is pushed by hand. However, enabling the adaptive control signal quickly stabilizes the overall system. When two additional pushes are applied, the control system with the adaptive control augmented shows that it well maintains stability and remains effective in damping vibrations in the base. Commanding a step change from 10 to 20 deg also leads to good performance in both tracking the step change in the joint angle and damping the vibrations in the base with this configuration. The existing inertial damping controller goes unstable with the same reference command.

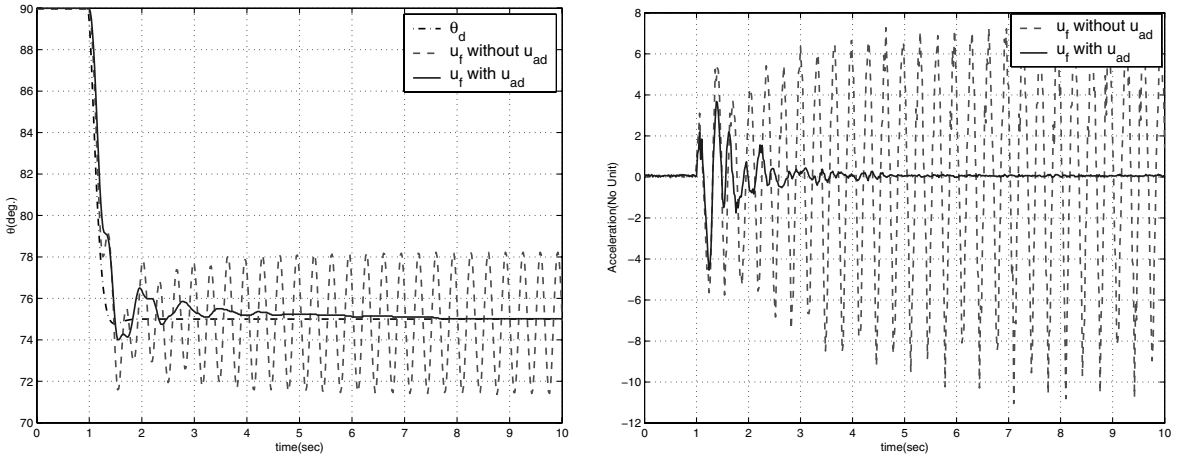

a) b)

Fig. 13 Responses a) of the joint angle and b) of the base acceleration, with increased inertia of 10.5585 kg.

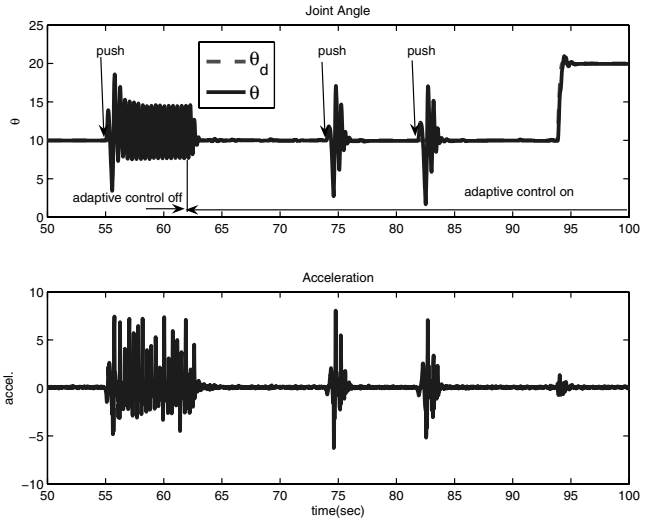

Fig. 15 The performance of adaptive control subjective impulsive disturbance and the tracking with the configuration in Fig. 14.

VII. Conclusions

The paper addresses neural network-based adaptive output feedback augmentation of an existing combined position and vibration control system for a flexible base manipulator. The approach modifies a previous method so that it is suitable for augmenting a previously designed two-time-scale controller in the application. Both the nonadaptive and the adaptive controllers with damping control are effective in reducing the transient time of the vibration. However, in steady state, only with adaptation can the micromanipulator achieve a level of accuracy on the order of the encoder resolution. In this case, adaptation overcomes the effects of actuation nonlinearities due to dead zone and stiction and provides highly accurate tip positioning. When mass variations are made at the tip of the manipulator or when the manipulator is operated outside of its nominal configuration, the closed-loop system using the exiting control exhibits instability, whereas the adaptively augmented system maintains nominal performance.

Appendix: Stability Analysis

The term $u_{nn} - \Delta_1$ in (22) allows for the following upper bound [41]:

$$|u_{nn} - \Delta_1| \le \alpha_1 \|\tilde{Z}\|_F + \alpha_2, \qquad c_1, c_2 > 0 \tag{A1}$$

where the subscript F denotes the Frobenius norm. Using Taylor series expansion, the NN approximation error $u_{nn} - \Delta_1$ can be represented as [33]

$$u_{nn} - \Delta_1 = \tilde{M}(\hat{\sigma} - \hat{\sigma}'\hat{N}^T\eta) + \hat{M}^T\hat{\sigma}'\tilde{N}^T\eta + \omega - \varepsilon \tag{A2}$$

where $\omega = \tilde{M}^T\hat{\sigma}'N^T\eta - M^T\mathcal{O}(\tilde{N}^T\eta)^2$. Using the bound for η in (28), the term $\omega - \varepsilon$ can be bounded [41]

$$\|\omega - \varepsilon\| \le \gamma_1\|\tilde{Z}\|_F + \gamma_2, \qquad \gamma_1, \gamma_2 > 0 \tag{A3}$$

Using the bound in (15), the bound in (9) can be written

$$\begin{aligned}\|\phi_2\| &\le \beta_0\{\|E\| + \beta_3\} + \beta_1\|z_2\| + \beta_2 \\ &\le \beta_0|e| + \beta_0\|\mu\| + \beta_1\|z_2\| + \delta_1\end{aligned} \tag{A4}$$

where $\delta_1 = \beta_0\beta_3 + \beta_2$, and $\mu = [\,\tilde{z}_1^T \quad x_{dc}^T\,]^T$. Note that the conservative bound $\|\tilde{z}_1\| \le \|\mu\|$ is used for simplicity of analysis. Similarly, the relation in (11) can also be upper bounded

$$\begin{aligned}\dot{V}_{z_2} &\le -\frac{3c_3}{4}\|z_2\|^2 + \frac{(c_4c_5)^2}{c_3}\|x\|^2 \\ &\le -\frac{3c_3}{4}\|z_2\|^2 + \frac{(c_4c_5)^2}{c_3}\|E\|^2 + \frac{(c_4c_5)^2}{c_3}\beta_3^2 \\ &\le -\frac{3c_3}{4}\|z_2\|^2 + \frac{(c_4c_5)^2}{c_3}[|e|^2 + \|\mu\|^2] + \frac{(c_4c_5)^2}{c_3}\beta_3^2\end{aligned} \tag{A5}$$

Suppose that β_is and c_is in (A4) and (A5), respectively, are such that Q in (24) can be chosen to satisfy

$$Q_m > 2\max\{C_1, C_2\} \tag{A6}$$

where $Q_m = \lambda_{\min}(Q)$, and C_1 and C_2 are defined as

$$\begin{aligned}C_1 &= \beta_0[3\|p_{21}\| + \|P_{22}B_\mu\|] \\ &\quad + \gamma_1|p_{11}b| + \frac{(2\beta_1\|p_{21}\|)^2 + (c_4c_5)^2}{c_3}, \\ C_2 &= \beta_0[\|p_{21}\| + 3\|P_{22}B_\mu\|] + \alpha_1\|p_{21}b\| \\ &\quad + \frac{(2\beta_1\|p_{21}\|)^2 + (c_4c_5)^2}{c_3}\end{aligned} \tag{A7}$$

in which $B_\mu = [\,I_{(m-1)\times(m-1)} \quad 0^T_{n_{dc}\times(m-1)}\,]^T$. Finally, let the σ-modification gain satisfy the following lower bound:

$$k > 2[\gamma_1|p_{11}b| + \alpha_1\|p_{21}b\|] \tag{A8}$$

Proof of Theorem 2. Consider the Lyapunov function candidate in (34). With (24), the time derivative $\dot{V}$ along with (22) will be

$$\begin{aligned}\dot{V} &= -E_a^TQ_aE_a + 2E_a^TP\begin{bmatrix}\bar{b}\\0\end{bmatrix}(u_{nn} - \Delta_1) \\ &\quad - 2E_a^TP\begin{bmatrix}B_2\\0\end{bmatrix}\phi_2 + \tilde{M}^T\Gamma_M^{-1}\dot{\hat{M}} + tr(\tilde{N}^TV^{-1}\dot{\hat{N}}) + \dot{V}_{z_2}\end{aligned} \tag{A9}$$

Using (A2), $\dot{V}$ can be written as

$$\begin{aligned}\dot{V} &= -E_a^TQ_aE_a + 2ep_{11}b[\tilde{M}(\hat{\sigma} - \hat{\sigma}'\hat{N}^T\eta) + \hat{M}^T\hat{\sigma}'\tilde{N}^T\eta + \omega - \varepsilon] \\ &\quad + 2\mu^Tp_{21}b[u_{nn} - \Delta_1] - 2ep_{21}^T\phi_2 - 2\mu^TP_{22}B_\mu\phi_2 \\ &\quad + \tilde{M}^T\Gamma_M^{-1}\dot{\hat{M}} + tr(\tilde{N}^TV^{-1}\dot{\hat{N}}) + \dot{V}_{z_2}\end{aligned} \tag{A10}$$

After substituting the adaptive law in (30), we have

$$\begin{aligned}\dot{V} &= -E_a^TQ_aE_a + 2ep_{11}b[\omega - \varepsilon] + 2\mu^Tp_{21}b[u_{nn} - \Delta_1] \\ &\quad - 2ep_{21}^T\phi_2 - 2\mu^TP_{22}B_\mu\phi_2 - k\tilde{M}^T\hat{M} - k\mathrm{tr}(\tilde{N}^T\hat{N}) + \dot{V}_{z_2}\end{aligned} \tag{A11}$$

Using upper bounds from (A1) and (A3–A5), $\dot{V}$ can be upper bounded as

$$\begin{aligned}\dot{V} &\le -Q_m\|E_a\|^2 + 2|e||p_{11}b|[\gamma_1\|\tilde{Z}\|_F + \gamma_2] \\ &\quad + 2\|\mu\|\|p_{21}b\|[\alpha_1\|\tilde{Z}\|_F + \alpha_2] \\ &\quad + 2\{|e|\|p_{21}\| + \|\mu\|\,\|P_{22}B_\mu\|\}[\beta_0|e| + \beta_0\|\mu\| \\ &\quad + \beta_1\|z_2\| + \delta_1] - (k/2)\|\tilde{Z}\|_F^2 - (3c_3/4)\|z_2\|^2 \\ &\quad + [(c_4c_5)^2/c_3][|e|^2 + \|\mu\|^2] + \bar{Z} + [(c_4c_5)^2/c_3]\beta_3^2\end{aligned} \tag{A12}$$

where $\bar{Z} = (k/2)[\|M - M_0\|_F^2 + \|N - N_0\|_F^2]$, and the following property for matrices has been used:

$$\mathrm{tr}\,[\tilde{N}^T(\hat{N} - N_0)] = \tfrac{1}{2}\|\tilde{N}\|_F^2 + \tfrac{1}{2}\|\hat{N} - N_0\|_F^2 - \tfrac{1}{2}\|N - N_0\|_F^2$$

Grouping terms leads to

$$\dot{V} \le -\left\{Q_m - 2\beta_0\|\boldsymbol{p}_{21}\| - \frac{(c_4c_5)^2}{c_3}\right\}|e|^2 + 2\theta_1|e|\,\|\boldsymbol{\mu}\| + 2\theta_2|e|\,\|z_2\| + 2s_1|e|\,\|\tilde{Z}\|_F + 2s_2|e| - \left\{Q_m - 2\beta_0\|P_{22}B_\mu\| - \frac{(c_4c_5)^2}{c_3}\right\}\|\boldsymbol{\mu}\|^2 + 2\theta_3\|\boldsymbol{\mu}\|\,\|z_2\| + 2\pi_1\|\boldsymbol{\mu}\|\,\|\tilde{Z}\|_F + 2\pi_2\|\boldsymbol{\mu}\| - \frac{3c_3}{4}\|z_2\|^2 - \frac{k}{2}\|\tilde{Z}\|_F^2 + \bar{Z} + \frac{(c_4c_5)^2}{c_3}\beta_3^2 \tag{A13}$$

where

$$\theta_1 = \beta_0[\|\boldsymbol{p}_{21}\| + \|P_{22}B_\mu\|], \qquad \theta_2 = \beta_1\|\boldsymbol{p}_{21}\|$$
$$\theta_3 = \beta_1\|P_{22}B_\mu\|, \qquad s_1 = \gamma_1|p_{11}b|$$
$$s_2 = \gamma_2|p_{11}b| + \delta_1\|\boldsymbol{p}_{21}\|, \qquad \pi_1 = \alpha_1\|\boldsymbol{p}_{21}b\|$$
$$\pi_2 = \alpha_2\|\boldsymbol{p}_{21}b\| + \delta_1\|P_{22}B_\mu\| \tag{A14}$$

The following upper bounds for product terms and linear terms

$$2\theta_1|e|\,\|\boldsymbol{\mu}\| \le \theta_1[|e|^2 + \|\boldsymbol{\mu}\|^2],$$
$$2s_2|e| \le (Q_m/2)|e|^2 + (2/Q_m)s_2^2 \tag{A15}$$

together with the following upper bound

$$-(c_3/4)\|z_2\|^2 + 2\theta_2|e|\|z_2\| \le [(2\theta_2)^2/c_3]|e|^2 \tag{A16}$$

leads to

$$\dot{V} \le -\kappa_{\boldsymbol{E}_a}\|\boldsymbol{E}_a\|^2 - (c_3/4)\|z_2\|^2 - \kappa_{\tilde{Z}}\|\tilde{Z}\|_F^2 + \Upsilon \tag{A17}$$

where $\kappa_{\boldsymbol{E}_a} = \min(\kappa_e, \kappa_{\boldsymbol{\mu}})$, and

$$\kappa_e = \frac{Q_m}{2} - \{\theta_1 + s_1 + 2\beta_0\|\boldsymbol{p}_{21}\|\} - \frac{(2\theta_2)^2 + (c_4c_5)^2}{c_3},$$
$$\kappa_{\boldsymbol{\mu}} = \frac{Q_m}{2} - \{\theta_1 + \pi_1 + 2\beta_0\|P_{22}B_\mu\|\} - \frac{(2\theta_2)^2 + (c_4c_5)^2}{c_3}, \tag{A18}$$
$$\kappa_{\tilde{Z}} = \frac{k}{2} - \{s_1 + \pi_1\}, \qquad \Upsilon = \bar{Z} + \frac{(c_4c_5)^2}{c_3}\beta_3^2 + \frac{2}{Q_m}[s_2^2 + \pi_2^2]$$

One of the following conditions

$$\|\boldsymbol{E}_a\| \ge \sqrt{\Upsilon/\kappa_{\boldsymbol{E}_a}}, \qquad \|z_2\| \ge 2\sqrt{\Upsilon/c_3}, \qquad \|\tilde{Z}\|_F \ge \sqrt{\Upsilon/\kappa_{\tilde{Z}}} \tag{A19}$$

will render $\dot{V} \le 0$ outside a compact set. To complete the proof, define

$$\gamma \triangleq \max\left\{\sqrt{\Upsilon/\kappa_{\boldsymbol{E}_a}}, 2\sqrt{\Upsilon/c_3}, \sqrt{\Upsilon/\kappa_{\tilde{Z}}}\right\} \tag{A20}$$

and consider the hypersphere

$$B_\gamma = \{\boldsymbol{\zeta} \in B_R | \|\boldsymbol{\zeta}\| \le \gamma\}$$

in the space of the error vector $\boldsymbol{\zeta}$ outside of which $\dot{V}(\boldsymbol{\zeta}) < 0$. Notice from (39), that $B_\gamma \subset B_R$. Let

$$\alpha_m \triangleq \max_{\|\boldsymbol{\zeta}\|=\gamma} \boldsymbol{\zeta}^T T_2 \boldsymbol{\zeta}^T = \gamma^2 T_{2_M}$$

and introduce the set:

$$\Omega_{\alpha_m} = \{\boldsymbol{\zeta} | \boldsymbol{\zeta}^T T_2 \boldsymbol{\zeta} \le \alpha_m\}$$

The condition in (39) ensures that $\Omega_{\alpha_m} \subset \Omega_{\alpha_M}$. Thus, if the initial error $\boldsymbol{\zeta}_0 = \boldsymbol{\zeta}(0)$ belongs to Ω_{α_M}, then there exists a time instant $t_\zeta(\boldsymbol{\zeta}_0)$, such that $\boldsymbol{\zeta}(t)$ will enter the set Ω_γ at t_ζ and remain thereafter. This implies uniform ultimate boundedness of $\boldsymbol{\zeta}$ and completes the proof. □

Acknowledgments

This research is supported by the U.S. Air Force Office of Scientific Research, under Grant No. FA9550-04-1-0165. The authors thank Wayne J. Book and Ryan Krauss in the School of Mechanical Engineering at Georgia Tech for allowing use of Small Articulated Manipulator II for this research and for many useful discussions. Figures 2 and 3 were also provided by them for use in this paper.

References

[1] Torres, M. A., and Dubowsky, S., "Path Planning for Elastically Constrained Space Manipulator Systems," *Institute of Electrical and Electronics Engineers International Conference on Robotics and Automation*, Vol. 1, IEEE Publications, Los Alamitos, CA, 1993, pp. 812–817.

[2] Dubowsky, S., "Dealing with Vibrations in the Deployment Structures of Space Robotic Systems," *Proceedings of the 5th International Conference on Adaptive Structures*, Technomic, Lancaster, PA, 1994, pp. 5–7.

[3] Meggiolaro, M., and Dubowsky, S., "Improving the Positioning Accuracy of Powerful Manipulators with Application in Nuclear Maintenance," *Proceedings of the 16th Brazilian Congress of Mechanical Engineering on Robotics and Control*, Vol. 15, Brazilian Society of Mechanical Sciences, Rio de Janeiro, Brazil, 2001, pp. 210–219.

[4] Jansen, J., Burks, B., Babcock, S., Kress, R., and Hamel, W., "Long-Reach Manipulator for Waste Storage Tank Remediation," *Proceedings of the American Society of Mechanical Engineers Winter Annual Meeting: Dynamic Systems and Control Division*, Vol. 1, American Society of Mechanical Engineers, New York, 1991, pp. 67–73.

[5] Longman, R., "Tutorial Overview of the Dynamics and Control of Satellite-Mounted Robots," *Teleoperation and Robotics in Space*, edited by S. Skaar and C. Ruoff, AIAA, Washington, D.C., 1994.

[6] Scott, M. G. G., and Demeo, M., "Active Vibration Damping of the Space Shuttle Remote Manipulator System," *Journal of Guidance, Control, and Dynamics*, Vol. 16, No. 2, 1993, pp. 275–280.

[7] Benosman, M., and Le Vey, G., "Control of Flexible Manipulators: A Survey," *Robotica*, Vol. 22, No. 5, 2004, pp. 533–545.

[8] Dwivedy, S., and Eberhard, P., "Dynamic Analysis of Flexible Manipulators: A Literature Review," *Mechanism and Machine Theory*, Vol. 41, No. 7, 2006, pp. 749–777.

[9] Singer, N., and Seering, W., "Preshaping Command Inputs to Reduce System Vibration," *Journal of Dynamic Systems, Measurement, and Control*, Vol. 112, No. 1, 1990, pp. 76–82.

[10] Meckl, P., "Robust Motion Control of Flexible Systems Using Feedforward Forcing Functions," *IEEE Transactions on Control Systems Technology*, Vol. 2, No. 3, 1994, pp. 245–253.

[11] Torres, M. A., Dubowsky, S., and Pisoni, A., "Path Planning for Elastically Mounted Space Manipulators: Experimental Evaluation of the Coupling Map," *Institute of Electrical and Electronics Engineers International Conference on Robotics and Automation*, IEEE Publications, Los Alamitos, CA, 1994, pp. 2227–2233.

[12] Magee, D. P., and Book, W. J., "Filtering Micro-Manipulator Writs Commands to Prevent Flexible Base Motion," *Proceedings of the American Control Conference*, Vol. 1, American Automatic Control Council, New York, 1995, pp. 924–928.

[13] Zuo, K., Drapeau, V., and Wang, D., "Closed Loop Shaped Input Strategies," *International Journal of Robotics Research*, Vol. 14, No. 5, 1995, pp. 510–529.

[14] Magee, D. P., Cannon, D. W., and Book, W. J., "Combined Command Shaping and Inertial Damping for Flexure Control," *Proceedings of the American Control Conference*, American Automatic Control Council, New York, 1997, pp. 1330–1334.

[15] Romano, M., Agrawal, B., and, Bernelli-Zazzera, F, "Experiments on Command Shaping Control of a Manipulator with Flexible Links," *Journal of Guidance, Control, and Dynamics*, Vol. 25, No. 2, March–April 2002, pp. 232–239.

[16] Staehlin, U., and Singh, T., "Design of Closed-Loop Input Shaping Controllers," *Proceedings of the American Control Conference*, Vol. 6, American Automatic Control Council, New York, 2003, pp. 5167–5172.

[17] Sharon, A., Hogan, N., and Hardt, D., "The Macro/Micro Manipulator: An Improved Architecture for Robot Control," *Robotics and Computer Integrated Manufacturing*, Vol. 10, No. 3, 1993, pp. 209–222.

[18] Pond, B., Van Vliet, J., and Sharf, I., "Prediction Tools for Active Damping and Motion Planning of Flexible Manipulators," *Journal of*

Guidance, Control, and Dynamics, Vol. 26, No. 2, March–April 2003, pp. 267–272.

[19] Ballhaus, W., and Rock, S., "End-Point Control of a Two-Link Flexible Robotic Manipulator with a Mini-Manipulator: Coupling Issues," *Dynamics of Flexible Multibody Systems: Theory and Experiment; Proceedings of the American Society of Mechanical Engineers Winter Annual Meeting*, American Society of Mechanical Engineers, New York, 1992, pp. 17–22.

[20] Stevens, H., and How, J., "Limitations of Independent Controller Design for a Multiple-Link Flexible Macro-Manipulator Carrying a Rigid Mini-Manipulator," *Proceedings of the 2nd American Society of Civil Engineers Conference on Robotics for Challenging Environment*, American Society of Civil Engineers, New York, 1996, pp. 93–99.

[21] Trudnowski, D. J., Baker, C., and Evans, M., "Damping Control of Large Flexible Manipulator Through Inertial Forces of a Small Manipulator," *Proceedings of the American Control Conference*, American Automatic Control Council, New York, 1993, pp. 2878–2879.

[22] Cannon, D., Magee, D., and Book, W., "Experimental Study on Micro/Macro Manipulator Vibration Control," *Institute of Electrical and Electronics Engineers International Conference on Robotics and Automation*, Institute of Electrical and Electronics Engineers Publications, New York, 1996, pp. 2549–2554.

[23] Lew, J., and Trudnowski, D. J., "Vibration Control of a Micro/Macro-Manipulator System," *IEEE Control Systems Magazine*, Vol. 16, No. 1, 1996, pp. 26–31.

[24] Sharf, I., "Active Damping of a Large Flexible Manipulator with a Short-Reach Robot," *Journal of Dynamic Systems, Measurement, and Control*, Vol. 118, No. 4, 1996, pp. 704–713.

[25] Magee, D. P., Cannon, D. W., and Book, W. J., "Inverse Dynamics for Commanding Micromanipulator Inertial Forces to Damp Macro-manipulator Vibration," *Proceedings of Institute of Electrical and Electronics Engineers/Robotics Society of Japan International Conference on Intelligent Robots and Systems*, IEEE Publications, Piscataway, NJ, 1997, pp. 1330–1334.

[26] Loper, J. C., "Vibration Cancellation and Disturbance Rejection in Serially Linked Micro/Macro Manipulators," Master's Thesis, School of Mechanical Engineering, Georgia Institute of Technology, Atlanta, GA, March 1998.

[27] Book, W., and Loper, J., "Inverse Dynamics for Commanding Micromanipulator Inertial Force to Damp Macromanipulator Vibration," *Proceedings of Institute of Electrical and Electronics Engineers/Robotics Society of Japan International Conference on Intelligent Robots and Systems*, IEEE Publications, Piscataway, NJ, 1999.

[28] George, L., and Book, W. J., "Inertial Vibration Damping Control of a Flexible Base Manipulator," *IEEE/ASME Transactions on Mechatronics*, Vol. 8, No. 2, 2003, pp. 268–271.

[29] Krauss, R., and Book, W. J., "Stability in Active Mass Damping Control of a Flexible Robot," *2004 Institute of Electrical and Electronics Engineers Aerospace Conference Proceedings*, IEEE Publications, Piscataway, NJ, 2004, pp. 2903–2911.

[30] George, L. E., "Active Vibration Control of a Flexible Base Manipulator," Ph.D. Thesis, Georgia Institute of Technology, School of Mechanical Engineering, Atlanta, GA, 2002.

[31] Hornik, N., Stinchcombe, M., and White, H., "Multilayer Feedforward Networks Are Universal Approximators," *Neural Networks*, Vol. 2, No. 5, 1989, pp. 359–366.

[32] Ge, S., Lee, T., and Harris, C., *Adaptive Neural Network Control of Robotic Manipulators*, World Scientific, River Edge, NJ, 1998.

[33] Lewis, F., Jagannathan, S., and Yeşildirek, A., *Neural Network Control of Robot Manipulators and Nonlinear Systems*, Taylor & Francis, London, 1999.

[34] Spooner, J. T., Maggiore, M., Ordóñez, R., and Passino, K. M., *Stable Adaptive Control and Estimation for Nonlinear Systems: Neural and Fuzzy Approximator Techniques*, John Wiley & Sons, New York, NY, 2002.

[35] Ge, S., Hang, C., Lee, T., and Zhang, T., *Stable Adaptive Neural Network Control*, Kluwer Academic, Boston, 2002.

[36] KrishnaKumar, K., and Montgomery, L., "Adaptive Neuro-Control for Large Flexible Structures," *Smart Materials and Structures*, Vol. 1, No. 4, 1992, pp. 312–323.

[37] Rao, V., Damle, R., Tebbe, C., and Kern, F., "Adaptive Control of Smart Structures Using Neural Networks," *Smart Materials and Structures*, Vol. 3, No. 3, 1994, pp. 354–366.

[38] Isogai, M., Arai, F., and Fukuda, T., "Modeling and Vibration Control with Neural Network for Flexible Multi-Link Structures," *Institute of Electrical and Electronics Engineers International Conference on Robotics and Automation*, IEEE Publications, Los Alamitos, CA, 1999, pp. 1096–1101.

[39] Gutiérrez, L., Lewis, F., and Lowe, A., "Implementation of a Neural Network Tracking Controller for a Single Flexible Link: Comparison with PD and PID Controllers," *IEEE Transactions on Industrial Electronics*, Vol. 45, No. 2, April 1998, pp. 307–318.

[40] Calise, A., Hovakimyan, N., and Idan, M., "Adaptive Output Feedback Control of Nonlinear Systems Using Neural Networks," *Automatica*, Vol. 37, No. 8, 2001, pp. 1201–1211.

[41] Hovakimyan, N., Nardi, F., Kim, N., and Calise, A., "Adaptive Output Feedback Control of Uncertain Systems Using Single Hidden Layer Neural Networks," *IEEE Transactions on Neural Networks*, Vol. 13, No. 6, 2002, pp. 1420–1431.

[42] Calise, A., Yang, B.-J., and Craig, J., "Augmenting Adaptive Approach to Control of Flexible Systems," *Journal of Guidance, Control, and Dynamics*, Vol. 27, No. 3, 2004, pp. 387–396.

[43] Hovakimyan, N., Yang, B.-J., and Calise, A., "Adaptive Output Feedback Control Methodology for Non-Minimum Phase Systems," *Proceedings of Conference on Decision and Control*, IEEE Publications, Piscataway, NJ, 2002, pp. 949–954.

[44] Hovakimyan, N., Yang, B.-J., and Calise, A. J., "Adaptive Output Feedback Control Methodology Applicable to Non-Minimum Phase Nonlinear Systems," *Automatica*, Vol. 42, No. 4, April 2006, pp. 513–522.

[45] Yang, B.-J., Hovakimyan, N., Calise, A., and Craig, J., "Experimental Validation of an Augmenting Approach to Adaptive Control of Uncertain Nonlinear Systems," AIAA 2003-5715, 2003.

[46] Moallem, M., Patel, R., and Khorasani, K., *Flexible-Link Robot Manipulators: Control Techniques and Structural Design*, Vol. 257, Lecture Notes in Control and Information Sciences, Springer–Verlag, London, 2000.

[47] Heintze, J., van Schothorst, G., van–der–Weiden, A. J. J., and Teerhuis, P.C., "Modeling and Control of an Industrial Hydraulic Rotary Vane Actuator," *Proceedings of Conference on Decision and Control*, IEEE Publications, Piscataway, NJ, 1993, pp. 1913–1918.

[48] Krauss, R., Brüls, O., and Book, W. J., "Two Competing Linear Models for Flexible Robots: Comparison, Experimental Validation, and Refinement," *Proceedings of the American Control Conference*, American Automatic Control Council, New York, 2005, pp. 1963–1968.

[49] Kutay, A. T., Fowler, J. M., Calise, A. J., and D'Andrea, R., "Distributed Adaptive Output Feedback Control Design and Application to a Formation Flight Experiment," *Proceedings of AIAA Guidance, Navigation and Control Conference*, AIAA, Reston, VA, 2005; AIAA Paper 2005-6368.

[50] Isidori, A., *Nonlinear Control Systems*, 3rd ed., Springer–Verlag, Berlin, 1995.

[51] Khalil, H., *Nonlinear Systems*, Prentice–Hall, Upper Saddle River, NJ, 1996.

[52] Lavretsky, E., Hovakimyan, N., and Calise, A., "Upper Bounds for Approximation of Continuous-Time Dynamics Using Delayed Outputs and Feedforward Neural Networks," *IEEE Transactions on Automatic Control*, Vol. 48, No. 9, 2003, pp. 1606–1610.